

RADIATION CHARACTERISTICS OF AN AXIALLY ASYMMETRICAL SLOT ANTENNA ON A PERFECTLY-CONDUCTING PROLATE SPHEROID COATED WITH HOMOGENEOUS MATERIALS

M. Zhang

Electromagnetics and Compatibility Group
Terrestrial Wireless System Research Branch
Communications Research Centre Canada
Ottawa, Ontario, K2H 8S2, Canada

A. A. Sebak

Department of Electrical and Computer Engineering
Concordia University
Montreal, Quebec, H4B 1R6, Canada

Abstract—The boundary value solution of electromagnetic radiation from an axis-asymmetric slot antenna on a perfectly conducting prolate spheroid coated with a confocal sheath is presented. The electromagnetic fields are expanded in terms of prolate spheroidal vector wave functions. The unknown expansion coefficients are determined from a set of linear equations derived from the application of boundary conditions on the tangential fields' components. Numerical results for radiation patterns and power are presented. It is found that the thickness of the sheath has a significant effect on the radiated fields, and the radiated power is greatly enhanced for certain values of the sheath thickness.

1 Introduction

2 Formulation of the Problem

- 2.1 Geometry
- 2.2 Spheroidal Wave Functions
- 2.3 Excitation Field
- 2.4 Radiated and Transmitted Fields

2.5 Formation of Boundary Conditions

2.6 Radiation Patterns and Power

3 Numerical Computation and Results

3.1 Radiation Patterns

3.2 Radiated Power

4 Conclusion

References

1. INTRODUCTION

The analysis of spheroidal antennas can be applied to the modeling of antennas with a variety of different geometries [1–7]. For example, the analysis of spheroidal antennas with a confocal sheath is helpful in the understanding of the radiation from antennas mounted on an aircraft or a space shuttle, where the protection coating layer of the aircraft or a space shuttle can be modeled by a confocal sheath.

Perhaps one of the most notable contributions to spheroidal antennas is that of Schelkunoff [2], who analyzed the radiation from a prolate spheroidal antenna excited by a specified field over an axial symmetric gap on its surface. For this symmetric case, the field components are independent of the ϕ -coordinate and can be split into two groups that can be analyzed separately according to the applied fields on the gap. This leads to a simplified two-dimensional problem. Schelkunoff analyzed the case of spheroidal antenna excited by a voltage source between two halves of a spheroid, and calculated the input admittance of the antenna. Following Schelkunoff, other researchers further explored this type of spheroidal antenna. Weeks [3] and Wait [4] analyzed radiation from prolate spheroidal antennas with the excitation gap arbitrarily located along the spheroid, and also presented the solution for a prolate spheroid antenna coated with a confocal sheath. Do-Nhat and MacPhie [5] investigated the problem of an excitation gap with a finite width. The input admittance for the antenna was obtained and compared to those of circular cylindrical dipole antennas for three types of gap fields: Dirac's function, uniform and ultraspherical distributions. Most recently, Li et al. [6] revisited the antenna excited by a delta voltage across an infinitesimally narrow gap and enclosed in a confocal radome coated with two dielectric confocal layers. Zhang and Sebak [7] have presented an analytical solution for the radiation from an axially-asymmetrical slot antenna on a perfectly conducting prolate spheroid. In their work, the radiation fields were expanded in terms of prolate-spheroidal

vector wave functions. Using the boundary-matching technique over the excitation aperture, a system of equations was set up to solve for the unknown expansion coefficients. Numerical results for radiation patterns and conductance for various configurations of the spheroid were obtained.

In the present paper, the analysis of radiation from an axially asymmetric slot spheroidal antenna enclosed in a confocal dielectric sheath is developed. The approach is an analytic one and is based on separating the wave equation in the spheroidal coordinates. The spheroidal structure is centrally excited through a narrow slot with azimuthally sinusoidal source. The introduction of the coating region increases the mathematical difficulty in formulating the problem because of the dependency of the angular spheroidal functions on the properties of the medium. This work also investigates the effect of the thickness of the sheath on the radiated fields and the radiated power.

2. FORMULATION OF THE PROBLEM

2.1. Geometry

Consider the axially asymmetric slot spheroidal antenna enclosed in a confocal dielectric sheath, as illustrated in Figure 1. Using the conventional notation for the spheroidal coordinate system (ξ, η, ϕ) , the narrow slot is $2L(|\phi| \leq \phi_1)$ long and $2\Delta\eta$ wide, and located on the perfectly conducting spheroidal surface ξ_1 . From Figure 1, $\phi_1 (= 2L/b')$ is the subtended angle of the slot with respect to the z -axis, and b' is the local radius of the slot arc at the location of η_1 . The conducting surface ξ_1 is coated with a homogenous material layer (sheath) bounded on an outer confocal spheroidal surface specified by ξ_o . The relative permittivity and permeability of the material are ϵ_r and μ_r respectively. The semi-major and semi-minor axes of the conducting surface ξ_1 (or inner surface of the sheath) are a and b , and the semi-major and semi-minor axes of the confocal outer surface ξ_o are c and d , respectively. These two surfaces are confocal with the semi-interfocal distance F . It then follows that

$$\xi_1 = \frac{a}{F} = a(a^2 - b^2)^{-1/2}, \tag{1a}$$

$$\xi_o = \frac{c}{F} = c(c^2 - d^2)^{-1/2}. \tag{1b}$$

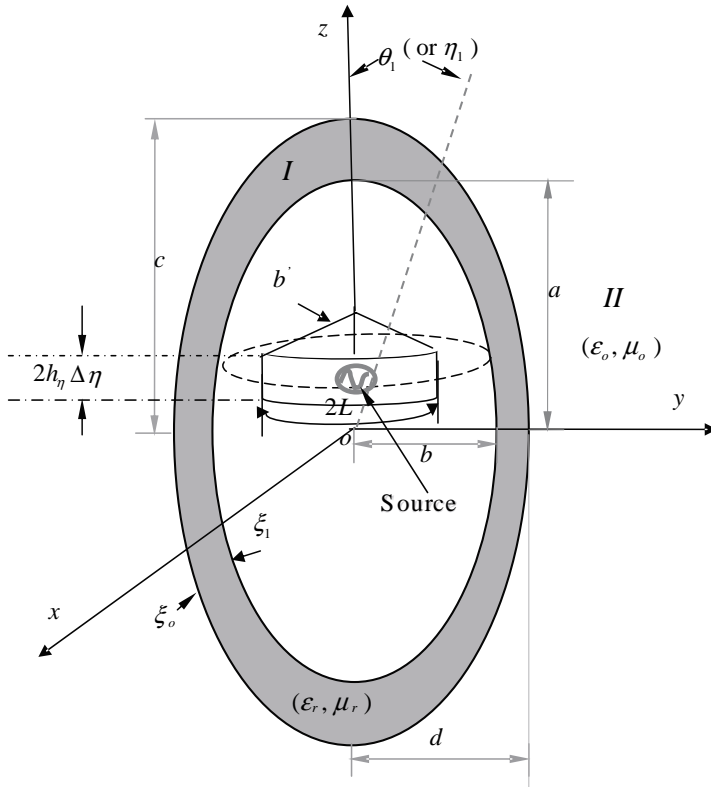


Figure 1. Geometry of axially asymmetric slot antenna on a perfectly conducting prolate spheroid with a homogeneous material confocal sheath.

The relation between the outer ratio of c/d and the inner ratio of a/b is given by

$$\frac{c}{d} = \frac{1}{\sqrt{1 - \left(\frac{a}{c}\right)^2 \left(1 - \left(\frac{b}{a}\right)^2\right)}}. \quad (2)$$

2.2. Spheroidal Wave Functions

The antenna with coating sheath, as shown in Figure 1, has two regions, namely the coating (sheath) region I ($\xi_1 \leq \xi \leq \xi_o$) and external region II ($\xi_o \leq \xi \leq \infty$). The electromagnetic fields in these regions satisfy Maxwell's vector wave equations, written as

Region I

$$\nabla^2 \vec{E} + k_1^2 \vec{E} = \vec{0}, \tag{3}$$

$$\nabla^2 \vec{H} + k_1^2 \vec{H} = \vec{0}, \tag{4}$$

Region II:

$$\nabla^2 \vec{E} + k_o^2 \vec{E} = \vec{0}, \tag{5}$$

$$\nabla^2 \vec{H} + k_o^2 \vec{H} = \vec{0}, \tag{6}$$

where k_o and k_1 are the wave numbers in free-space and the sheath. The electromagnetic fields in the above vector wave equations of (3)–(6) can be formed by solving the scalar wave equation in the spheroidal coordinate system

$$\nabla^2 \Psi + k^2 \Psi = 0 \tag{7}$$

The particular solutions of equation (7) can be obtained by using the separation of variable technique, expressed as [8]:

$$\Psi_{e_{m,n}}^{(j)} = S_{m,n}(h, \eta) R_{m,n}^{(j)}(h, \xi) \frac{\cos m\phi}{\sin m\phi}, \tag{8}$$

$S_{m,n}(h, \eta)$ and $R_{m,n}^{(j)}(h, \xi)$ are, respectively, the angular function and the j -th kind of radial function with order m and degree n , and $h = kF$. The superscript j may take the values of 1, 2, 3 or 4, representing one of the four kinds of radial functions [8]. The subscripts e and o refer to even and odd ϕ -dependence, respectively. In terms of the scalar wave functions given in (8), solutions for the vector wave equations of (3)–(6) in the spheroidal coordinates can be obtained as [8]:

$$\vec{M}_{e_{m,n}}^{\vec{q}(j)} = \nabla \Psi_{e_{m,n}}^{(j)} \times \hat{q} \tag{9}$$

$$\vec{N}_{e_{m,n}}^{\vec{q}(j)} = k^{-1} \nabla \times \vec{M}_{e_{m,n}}^{\vec{q}(j)} \tag{10}$$

where the vector \hat{q} is an arbitrary unit constant vector, which could be $\hat{x}, \hat{y}, \hat{z}$, or the unit position vector \hat{r} . Both vectors \vec{M} and \vec{N} are solenoidal.

2.3. Excitation Field

Assume that the narrow slot of Figure 1 is centrally excited with the electric field, which is polarized in the η -direction, and given as a

common sinusoidal form by:

$$E_{\eta}^{ex} = \begin{cases} \frac{V_o}{2h_{\eta_1}\Delta\eta} \sin[k_1(L-b'|\phi|)], & |b'\phi| \leq \phi, \eta_1 - \Delta\eta \leq \eta \leq \eta_1 + \Delta\eta \\ 0 & \text{otherwise} \end{cases} \quad (11)$$

where

$$h_{\eta_1} = F\sqrt{\frac{\xi_1^2 - \eta^2}{1 - \eta^2}}, \quad b' = F\sqrt{(1 - \eta_1^2)(\xi_1^2 - 1)}$$

and V_o is the voltage across the slot and $\Delta\eta$ is the slot width. The time dependent factor $e^{j\omega t}$ is assumed and suppressed throughout. To solve the problem in the spheroidal coordinate system, the excitation field E_{η}^{ex} is expanded in the following form,

$$E_{\eta}^{ex}(\eta, \phi) = \sum_{m=0}^{\infty} E_{\eta m}^{ex} \cos(m\phi), \quad (12)$$

where the expansion coefficients $E_{\eta m}^{ex}$ are given by

$$\begin{aligned} E_{\eta m}^{ex} &= \frac{V_0}{(1 + e_{m,0})\pi h_{\eta_1}(\Delta\eta)} \times \int_0^{L/b'} \sin[k_1(L - b'\phi)] \cos(m\phi) d\phi \\ &= \frac{V_0}{\pi h_{\eta_1}(\Delta\eta)} E_m, \quad (m = 0, 1, 2, \dots) \end{aligned} \quad (13)$$

with

$$E_m = \begin{cases} \frac{1}{k_1} [1 - \cos(k_1 L)], & m = 0 \\ \frac{2k_1 b'}{\pi [(k_1 b')^2 - m^2]} \left[\cos\left(m \frac{L}{b'}\right) - \cos(k_1 L) \right], & m \neq 0 \text{ or } k_1 b' \\ \frac{L}{b'} \sin(k_1 L), & m = k_1 b' \end{cases} \quad (14)$$

and

$$e_{m,0} = \begin{cases} 1 & m = 0 \\ 0 & m \neq 0 \end{cases}.$$

2.4. Radiated and Transmitted Fields

For the present problem, electromagnetic fields \vec{E} and \vec{H} are purely solenoidal, and may be expanded in terms of vector wave functions \vec{M}

and \vec{N} . This is analogous to radiating problems developed in spherical coordinates.

In Region II, the fields \vec{E} and \vec{H} are radiated fields, which must satisfy the radiation condition and have the same ϕ -dependency as the applied excitation field. Thus, the fourth kind of vector wave functions of $\vec{M}_{e_{o,m,n}}^{r(4)}$ and $\vec{N}_{e_{o,m,n}}^{r(4)}$ must be used. The radiated electric and magnetic fields are expressed as:

$$\vec{E}^R = \sum_{m=0}^{\infty} \sum_{n=m}^{\infty} \left[\gamma_{m,n} \vec{M}_{e_{o,m,n}}^{r(4)}(h_o, \xi, \eta, \phi) + \delta_{m,n} \vec{N}_{e_{o,m,n}}^{r(4)}(h_o, \xi, \eta, \phi) \right], \quad (15)$$

$$\vec{H}^R = \frac{j}{Z_o} \sum_{m=0}^{\infty} \sum_{n=m}^{\infty} \left[\gamma_{m,n} \vec{N}_{e_{o,m,n}}^{r(4)}(h_o, \xi, \eta, \phi) + \delta_{m,n} \vec{M}_{e_{o,m,n}}^{r(4)}(h_o, \xi, \eta, \phi) \right]. \quad (16)$$

$\gamma_{m,n}$ and $\delta_{m,n}$ are two unknown coefficients to be determined from boundary conditions, Z_o is the intrinsic impedance of free space and $j = \sqrt{-1}$. In the above expressions, functions $\vec{M}_{e_{o,m,n}}^{r(4)}$ and $\vec{N}_{e_{o,m,n}}^{r(4)}$ have been adopted by setting $\hat{q} = \hat{r}$ in (9) and (10). The reason for this selection is that the far-zone radiated fields should take similar forms to those in the corresponding spherical case. This may be verified by using asymptotic forms for $\vec{M}_{e_{o,m,n}}^{r(4)}$ and $\vec{N}_{e_{o,m,n}}^{r(4)}$ as $h_o \xi \rightarrow \infty$ in expressions (15) and (16) [8]. The far-radiated fields for the slotted antenna can then be written as

$$E_{\eta}^R = \frac{e^{-jk_o r}}{k_o r} \sum_{m=0}^{\infty} \sum_{n=m}^{\infty} j^n \left(-\frac{mj S_{m,n}(h_o, \cos \theta)}{\sin \theta} \gamma_{m,n} + \sin \theta \frac{dS_{m,n}(h_o, \cos \theta)}{d(\cos \theta)} \delta_{m,n} \right) \cos(m\phi) \quad (17a)$$

$$E_{\phi}^R = \frac{e^{-jk_o r}}{k_o r} \sum_{m=0}^{\infty} \sum_{n=m}^{\infty} j^n \left(j \sin \theta \frac{dS_{m,n}(h_o, \cos \theta)}{d \cos \theta} \gamma_{m,n} - \frac{m S_{m,n}(h_o, \cos \theta)}{\sin \theta} \delta_{m,n} \right) \sin(m\phi) \quad (17b)$$

$$H_{\eta}^R = -E_{\phi}^R / Z_o \quad (17c)$$

$$H_{\phi}^R = E_{\eta}^R / Z_o \quad (17d)$$

These forms are similar to those of the spherical case in the far-zone, except for the angular function $S_{m,n}(h_o, \eta)$.

In the sheath region ($\xi_1 \leq \xi \leq \xi_o$, Region I), the first and second spheroidal vector wave functions are both finite. The outgoing and

incoming waves must be taken into account. The transmitted fields may be expressed in the form,

$$\vec{E}^T = \sum_{m=0}^{\infty} \sum_{n=m}^{\infty} \left[\alpha_{m,n}^{(1)} \vec{M}_{m,n}^{r(1)}(h_1, \xi, \eta, \phi) + \beta_{m,n}^{(1)} \vec{N}_{m,n}^{r(1)}(h_1, \xi, \eta, \phi) + \alpha_{m,n}^{(2)} \vec{M}_{m,n}^{(2)}(h_1, \xi, \eta, \phi) + \beta_{m,n}^{(2)} \vec{N}_{m,n}^{(2)}(h_1, \xi, \eta, \phi) \right], \quad (18)$$

$$\vec{H}^T = \frac{j}{Z_1} \sum_{m=0}^{\infty} \sum_{n=0}^{\infty} \left[\alpha_{m,n}^{(1)} \vec{N}_{m,n}^{r(1)}(h_1, \xi, \eta, \phi) + \beta_{m,n}^{(1)} \vec{M}_{m,n}^{r(1)}(h_1, \xi, \eta, \phi) + \alpha_{m,n}^{(2)} \vec{N}_{m,n}^{(2)}(h_1, \xi, \eta, \phi) + \beta_{m,n}^{(2)} \vec{M}_{m,n}^{(2)}(h_1, \xi, \eta, \phi) \right], \quad (19)$$

where $\alpha_{m,n}^{(1)}$, $\beta_{m,n}^{(1)}$, $\alpha_{m,n}^{(2)}$ and $\beta_{m,n}^{(2)}$ are the unknown coefficients to be determined, $h_1 = k_1 F$ and $Z_1 = \sqrt{\frac{\mu}{\varepsilon}}$ is the intrinsic impedance of the sheath. In the above expression, the even (e) or odd (o) vector wave functions have been chosen according to the ϕ -dependence of the excitation fields, described in (12).

2.5. Formation of Boundary Conditions

The unknown expansion coefficients in the above expressions for the radiated fields, (15) and (16), and transmitted fields, (18) and (19), are determined by using the boundary conditions on both surfaces. Explicitly the conditions can be expressed as:

$$E_{\eta}^T = E_{\eta}^R \quad \text{and} \quad E_{\phi}^T = E_{\phi}^R, \quad \text{at} \quad \xi = \xi_o, \quad (20)$$

$$H_{\eta}^T = H_{\eta}^R \quad \text{and} \quad H_{\phi}^T = H_{\phi}^R, \quad \text{at} \quad \xi = \xi_o, \quad (21)$$

$$E_{\eta}^T = \begin{cases} E_{\eta}^{ex}, & \xi = \xi_1, \quad |b'\phi| \leq \phi \quad \text{and} \quad \eta_1 - \Delta\eta \leq \eta \leq \eta_1 + \Delta\eta \\ 0, & \text{Otherwise} \end{cases}, \quad (22)$$

and

$$E_{\phi}^T = 0 \quad \text{at} \quad \xi = \xi_1. \quad (23)$$

Substituting the field expressions (15), (16), (18) and (19) into these boundary conditions and applying the orthogonal properties of the trigonometric functions, a set of equations, for $m = 0, 1, 2, \dots$, involving series with unknown coefficients can be obtained. In this set of equations, each term is a complicated combination of the angular variable η , the spheroidal angular function $S_{m,n}(h, \eta)$, and

its derivative. This situation is quite similar to that in [7], but in the present case the complication arises due to the dependency of $S_{m,n}(h, \eta)$ on the properties of the sheath material. To set up a system of equations for the six unknown expansion coefficients $\alpha_{m,n}^{(1)}$, $\beta_{m,n}^{(1)}$, $\alpha_{m,n}^{(2)}$, $\beta_{m,n}^{(2)}$, $\gamma_{m,n}$ and $\delta_{m,n}$, we perform the following three steps:

- (1) Multiply the equations representing the continuity of η -components at the surface ξ_1 by the factor $(\xi_1^2 - \eta^2)^{5/2} S_{m+1, m+N+1}(h_1, \eta)$ and those at the surface ξ_o by the factor $(\xi_o^2 - \eta^2)^{5/2} S_{m+1, m+N+1}(h_1, \eta)$,
- (2) Multiply the equations representing the continuity of ϕ -components at the surface ξ_1 by the factor $(\xi_1^2 - \eta^2)(\xi_1^2 - 1)^{-1/2} S_{m+1, m+N+1}(h_1, \eta)$ and those at the surface ξ_o by the factor $(\xi_o^2 - \eta^2)(\xi_o^2 - 1)^{-1/2} S_{m+1, m+N+1}(h_1, \eta)$;
- (3) Integrate the resulting equations over η ($-1 \leq \eta \leq +1$) and use the quasi-orthogonality [8] of the spheroidal angular function $S_{m,n}(h, \eta)$ and the orthogonality of Legendre function.

From these steps, we obtain the following system of equations for the six unknown coefficients:

$$\begin{aligned} & \sum_{n=0}^{\infty} \left[\alpha_{m, m+n}^{(1)} A_{m, N, n}^{(1)}(h_1, h_1, \xi_1) + \beta_{m, m+n}^{(1)} B_{m, N, n}^{(1)}(h_1, h_1, \xi_1) \right. \\ & \left. + \alpha_{m, m+n}^{(2)} A_{m, N, n}^{(2)}(h_1, h_1, \xi_1) + \beta_{m, m+n}^{(2)} B_{m, N, n}^{(2)}(h_1, h_1, \xi_1) \right] \\ = & F_{m+1, m+N+1}(h_1, \xi_1) \end{aligned} \tag{24a}$$

$$\begin{aligned} & \sum_{n=0}^{\infty} \left[\alpha_{m, m+n}^{(1)} C_{m, N, n}^{(1)}(h_1, h_1, \xi_1) + \beta_{m, m+n}^{(1)} D_{m, N, n}^{(1)}(h_1, h_1, \xi_1) \right. \\ & \left. + \alpha_{m, m+n}^{(2)} C_{m, N, n}^{(2)}(h_1, h_1, \xi_1) + \beta_{m, m+n}^{(2)} D_{m, N, n}^{(2)}(h_1, h_1, \xi_1) \right] \\ = & 0 \end{aligned} \tag{24b}$$

$$\begin{aligned} & \sum_{n=0}^{\infty} \left[\alpha_{m, m+n}^{(1)} A_{m, N, n}^{(1)}(h_1, h_1, \xi_o) + \beta_{m, m+n}^{(1)} B_{m, N, n}^{(1)}(h_1, h_1, \xi_o) \right. \\ & \left. + \alpha_{m, m+n}^{(2)} A_{m, N, n}^{(2)}(h_1, h_1, \xi_o) + \beta_{m, m+n}^{(2)} B_{m, N, n}^{(2)}(h_1, h_1, \xi_o) \right] \\ = & \sum_{n=0}^{\infty} \left[\gamma_{m, m+n} A_{m, N, n}^{(4)}(h_o, h_1, \xi_o) + \delta_{m, m+n} B_{m, N, n}^{(4)}(h_o, h_1, \xi_o) \right] \tag{24c} \\ & \sum_{n=0}^{\infty} \left[\alpha_{m, m+n}^{(1)} C_{m, N, n}^{(1)}(h_1, h_1, \xi_o) + \beta_{m, m+n}^{(1)} D_{m, N, n}^{(1)}(h_1, h_1, \xi_o) \right] \end{aligned}$$

$$\begin{aligned}
 & + \alpha_{m,m+n}^{(2)} C_{m,N,n}^{(2)}(h_1, h_1, \xi_o) + \beta_{m,m+n}^{(2)} D_{m,N,n}^{(2)}(h_1, h_1, \xi_o) \Big] \\
 = & \sum_{n=0}^{\infty} \left[\gamma_{m,m+n} C_{m,N,n}^{(4)}(h_o, h_1, \xi_o) + \delta_{m,m+n} D_{m,N,n}^{(4)}(h_o, h_1, \xi_o) \right] \quad (24d)
 \end{aligned}$$

$$\begin{aligned}
 & Z_r \sum_{n=0}^{\infty} \left[\alpha_{m,m+n}^{(1)} B_{m,N,n}^{(1)}(h_1, h_1, \xi_o) - \beta_{m,m+n}^{(1)} A_{m,N,n}^{(1)}(h_1, h_1, \xi_o) \right. \\
 & \left. + \alpha_{m,m+n}^{(2)} B_{m,N,n}^{(2)}(h_1, h_1, \xi_o) - \beta_{m,m+n}^{(2)} A_{m,N,n}^{(2)}(h_1, h_1, \xi_o) \right] \\
 = & \sum_{n=0}^{\infty} \left[\gamma_{m,m+n} B_{m,N,n}^{(4)}(h_o, h_1, \xi_o) - \delta_{m,m+n} A_{m,N,n}^{(4)}(h_o, h_1, \xi_o) \right] \quad (24e)
 \end{aligned}$$

$$\begin{aligned}
 & Z_r \sum_{n=0}^{\infty} \left[-\alpha_{m,m+n}^{(1)} D_{m,N,n}^{(1)}(h_1, h_1, \xi_o) + \beta_{m,m+n}^{(1)} C_{m,N,n}^{(1)}(h_1, h_1, \xi_o) \right. \\
 & \left. - \alpha_{m,m+n}^{(2)} D_{m,N,n}^{(2)}(h_1, h_1, \xi_o) + \beta_{m,m+n}^{(2)} C_{m,N,n}^{(2)}(h_1, h_1, \xi_o) \right] \\
 = & \sum_{n=0}^{\infty} \left[-\gamma_{m,m+n} D_{m,N,n}^{(4)}(h_o, h_1, \xi_o) + \delta_{m,m+n} C_{m,N,n}^{(4)}(h_o, h_1, \xi_o) \right] \quad (24f)
 \end{aligned}$$

where $m, N = 0, 1, 2, \dots \infty$, $h_o = k_o F$, $h_1 = k_1 F$ and $Z_r = Z_o/Z_1 = \sqrt{\frac{\epsilon_r}{\mu_r}}$. The coefficients of A, B, C, D and F in the above system of equations can be calculated as:

$$\begin{aligned}
 A_{m,N,n}^{(j)}(x, y, \xi) &= -m\xi R_{m,m+n}^{(j)}(x, \xi) \\
 &\quad \cdot \left[(\xi^2 - 1)^2 I_{1mNn}(x, y) + 2(\xi^2 - 1) I_{2mNn}(x, y) \right], \quad (25) \\
 B_{m,N,n}^{(j)}(x, y, \xi) &= \frac{1}{x} \left\{ \left[(2\xi^2 - 1) R_{m,m+n}^{(j)}(x, \xi) \right. \right. \\
 &\quad \left. \left. + \xi(\xi^2 - 1) \frac{d}{d\xi} R_{m,m+n}^{(j)}(x, \xi) \right] \right. \\
 &\quad \times \left[(\xi^2 - 1) I_{4mNn}(x, y) + I_{5mNn}(x, y) \right] \\
 &\quad \left. - 2\xi^2(\xi^2 - 1) R_{m,m+n}^{(j)}(x, \xi) I_{4mNn}(x, y) \right. \\
 &\quad \left. + \left[(\lambda_{m,m+n}(x) - x^2 \xi^2)(\xi^2 - 1) + m^2 \right] \right. \\
 &\quad \left. \cdot R_{m,m+n}^{(j)}(x, \xi) - 2\xi(\xi^2 - 1) \frac{d}{d\xi} R_{m,m+n}^{(j)}(x, \xi) \right] \\
 &\quad \cdot I_{6mNn}(x, y) + \left[\lambda_{m,m+n}(x) - x^2 \xi^2 + \frac{m^2}{(\xi^2 - 1)} \right]
 \end{aligned}$$

$$\begin{aligned} & \cdot I_{7mNn}(x, y)R_{m,m+n}^{(j)}(x, \xi) \\ & + m^2 R_{m,m+n}^{(j)}(x, \xi) \left[(\xi^2 - 1)I_{8mNn}(x, y) \right. \\ & \left. + 2I_{6mNn}(x, y) + \frac{I_{7mNn}(x, y)}{(\xi^2 - 1)} \right] \}, \end{aligned} \tag{26}$$

$$\begin{aligned} C_{m,N,n}^{(j)}(x, y, \xi) &= \xi R_{m,m+n}^{(j)}(x, \xi)I_{4mNn}(x, y) \\ & - \frac{d}{d\xi} R_{m,m+n}^{(j)}(x, \xi)I_{6mNn}(x, y), \end{aligned} \tag{27}$$

$$\begin{aligned} D_{m,N,n}^{(j)}(x, y, \xi) &= -\frac{m}{x} \left\{ \left[\xi \frac{d}{d\xi} R_{m,m+n}^{(j)}(x, \xi) + R_{m,m+n}^{(j)}(x, \xi) \right] \right. \\ & \cdot I_{1mNn}(x, y) + \frac{R_{m,m+n}^{(j)}(x, \xi)}{(\xi^2 - 1)} [I_{9mNn}(x, y) \\ & \left. + I_{2mNn}(x, y) \right] \}, \end{aligned} \tag{28}$$

$$F_{m+1,m+N+1}(x, \xi) = - \int_{\eta_1 - \Delta\eta}^{\eta_1 + \Delta\eta} E_n^{ex}(\xi^2 - \eta^2)^{5/2} S_{m+1,m+N+1}(x, \eta) d\eta. \tag{29}$$

Where $x, y = h_1$ or h_o and $\lambda_{m,m+n}(x)$ is the eigenvalue of the spheroidal wave equation [8], and the superscript j indicates the j -th kind of spheroidal prolate radial functions and takes the values of 1, 2 and 4. The expressions for the integrals $I_{pmNn}(x, y)(p = 1, 2 \dots 9)$ are given in [9].

From (13), (29) can be written in the form

$$\begin{aligned} F_{m+1,m+N+1}(x, \xi) &= - \int_{\eta_1 - \Delta\eta}^{\eta_1 + \Delta\eta} \frac{V_o E_m}{x\pi \Delta\eta} \sqrt{(1 - \eta^2)} (\xi^2 - \eta^2)^2 \\ & \cdot S_{m+1,m+N+1}(x, \eta) d\eta, \end{aligned} \tag{30}$$

where the expansion E_m for the applied excitation is given in (14). For the case of the narrow slot ($\Delta\eta$ is very small), (30) can be expressed as

$$F_{m+1,m+N+1}(x, \xi) = - \frac{V_o E_m}{x\pi} \sqrt{(1 - \eta_1^2)} (\xi^2 - \eta_1^2)^2 S_{m+1,m+N+1}(x, \eta_1). \tag{31}$$

2.6. Radiation Patterns and Power

Once the coefficients $\alpha_{m,n}^{(1)}$, $\beta_{m,n}^{(1)}$, $\alpha_{m,n}^{(2)}$, $\beta_{m,n}^{(2)}$, $\gamma_{m,n}$ and $\delta_{m,n}$ are obtained, the transmitted fields in the sheath can be calculated by using (18) and (19), and the radiated fields by using (15) and (16). The radiation patterns can be obtained from the far-zone field asymptotic expressions (17a) and (17b) as $h_o\xi \rightarrow \infty$. To calculate the total radiated power from the antenna, the time-average radial components of the Poynting vector in free-space can be written as:

$$p = \frac{1}{2} \left(\vec{E}^R \times \vec{H}^{R*} \right) \cdot \hat{r} = \frac{1}{2Z_o} \left(|E_\eta^R|^2 + |E_\phi^R|^2 \right), \quad (32)$$

where as usual, \hat{r} is the unit vector in the radial direction. Integrating expression (32) over an infinitely large spherical surface centered at the antenna, the total radiated power can be expressed as:

$$P = \frac{1}{2Z_o k_o} \sum_{m=0}^{\infty} \sum_{n=0}^{\infty} \sum_{N=0}^{\infty} (1 + e_{m,0}) \left[\gamma_{m,m+n} \gamma_{m,m+N}^* + \delta_{m,m+n} \delta_{m,m+N}^* \right] \\ \times \left[\lambda_{m,m+n}(h_o) I_{10mnN}(h_o, h_o) - h_o^2 I_{11mnN}(h_o, h_o) \right], \quad (33)$$

where the symbol * denotes the complex conjugate, and the two integrals I_{10mnN} and I_{11mnN} have been evaluated in [9].

3. NUMERICAL COMPUTATION AND RESULTS

The scheme developed by Sinha and MacPhie [10] has been employed to compute eigenvalues $\lambda_{m,n}$ and the expansion coefficients $d_r^{mn}(h)$ and $a_r^{mn}(h)$ of the spheroidal angular and radial functions $S_{m,n}(h, \eta)$ and $R_{m,n}^{(j)}(h, \xi)$. In addition, the system of equations (24) for $\alpha_{m,n}^{(1)}$, $\beta_{m,n}^{(1)}$, $\alpha_{m,n}^{(2)}$, $\beta_{m,n}^{(2)}$, $\gamma_{m,n}$ and $\delta_{m,n}$ are also expressed in infinite series. However, in order to generate numerical results we must invert a matrix of infinite order. Therefore from practical point of view the series solution must be truncated in a suitable fashion to obtain a finite matrix by using an adequately large value N_o to achieve a convergent solution with a reasonable degree of accuracy. The choice of this number N_o was investigated by Sinha and MacPhie [10] and depends on the electrical size and property of each region. They theoretically and numerically shown that the amplitude of the spheroidal angular function dampens down sharply, when m, n , or $N > N_o$. They also showed that N_o depends on the maximum electrical size (wave number times the semi-major axis) of the spheroidal geometries, and is larger than or at least equal to the integral part of the maximum size plus 4.

The convergent criterion was also tested by Sebak and Sinha [11] by considering the scattering from a perfectly conducting spheroid coated with a confocal dielectric layer. In our case, to determine the value N_o , the maximum value between $k_o c$ and $k_1 a$ is firstly found, then the calculations are repeated for consecutive incremental values of n , commencing with the value stated by Sinha and MacPhie [10]. The evaluation is executed until an acceptable convergent solution with the required degree of accuracy is achieved.

To examine the accuracy of the solution, two types of numerical tests were considered. In the first type, the solution behavior over the boundary surface ξ_1 around the slot region, as given in (22), is checked; while in the other type we make comparison with the corresponding results of spherical structures, which can be considered as special cases of the spheroidal geometries.

The tangential component of the transmitted electric field E_η^T on the surface ξ_1 around the slot region was calculated using (18) for various parameters. Some of the results are shown in Figure 2. It is seen that the computed tangential component E_η^T matches the applied excitation field closely within the slot and only with slight ripples at the slot edges. This shows the correct behavior of the electric field on the boundary, and hence partially verifies the correctness of our solution from the point of view of the near field.

Mushiake [12] analyzed the radiation problem from an aperture (or an axial-asymmetric slot) on a perfectly conducting sphere, and presented the numerical results for the far-field patterns. His work provides another check for our solution in the far field zone. Consider the spheroidal case with a ratio of $a/b \approx 1$, as shown in Figure 1. This is a special case of a spheroidal antenna excited with electric field polarized in the θ -direction over an aperture (with length $2L = \lambda_o/2$). Furthermore, the sheath surrounding the antenna is assumed to be filled with material parameters of $\epsilon_r \approx 1$ and $\mu_r \approx 1$, and hence approximately transparent to free-space. This assumption, together with the special geometry, lead to a quasi-spherical slot antenna without coating, and excited with the same excitation source as given in (22). This antenna has been analyzed by Mushiake [12].

Figure 3 shows the calculated relative patterns of a half-wavelength ($2L = \lambda_o/2$) narrow slot antenna located at the equator ($\eta_1 = 0$ or $\theta_1 = 90^\circ$) on a perfectly conducting sphere without coating. Very good agreement can be found between Mushiake's results and ours for a range of parameters. This case together with the correct field distribution around the slot verifies the accuracy of our solution in both near and far field zones. Thus the solution can be used to analyze radiation from spheroidal antennas.

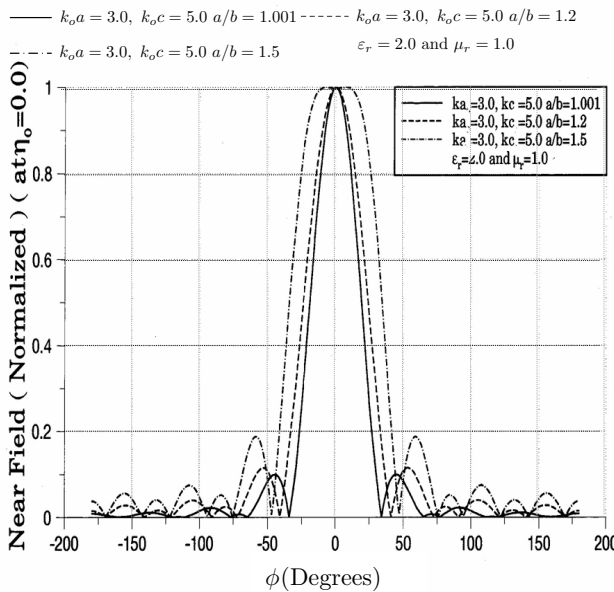


Figure 2. Tangential near electric field distribution around the slot located at $\eta_o = 0$ on the inner surface ξ_1 with the parameters: slot length $2L = \lambda_o/2$, $k_o a = 3.0$, $\mu_r = 1.0$ and the ratios $a/b = 1.001, 1.2$ and 1.5 . The half subtended angles of the slot with respect to these ratio are $|\phi_o| = \pi/6, \pi/5$ and $\pi/4$.

3.1. Radiation Patterns

The radiation patterns of the spheroidal half-wavelength slot antenna for various parameter combinations were obtained, some of these results being shown in Figures 4–6. These examples can be used to predict the effects of varying the material and geometric parameters on the radiation patterns. Figure 4 shows the patterns with a smaller ratio value of $a/c = 1/3$ (or a combination of electrical sizes $k_o a$ and $k_o c$). According to (2), increasing the ratios of a/b from 1.2 to 2 causes a small departure of the outer surface of the sheath from a spherical geometry (the outer ratio values of c/d is close to 1). These are the cases for the spheroidal antenna coated with approximately spherical sheath, their patterns vary from quasi-omni-directional, less-directional to wide-directional beams.

Figure 5 shows the radiation patterns with a larger value of $a/c = 0.6$, namely, almost twice the former value as given in Figure 4. This value, plus the increase in the values of a/b , configures the

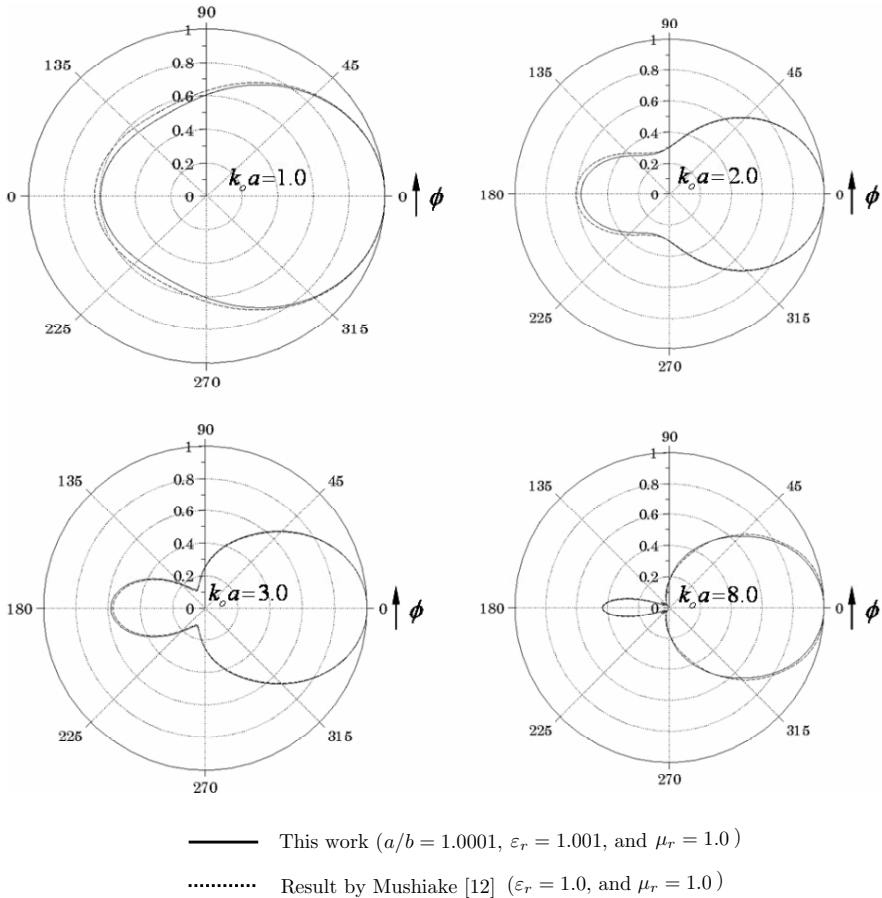


Figure 3. Radiation patterns of a half-wavelength narrow slot antenna on perfectly conducting quasi-sphere ($a/b = 1.0001$) in quasi-air ($\epsilon_r = 1.001$ and $\mu_r = 1.0$). The results calculated in reference [12] for a half-wavelength narrow slot antenna on perfectly conducting sphere are displayed as a comparison.

coating sheath more spheroidally. The radiation patterns for those configurations are significantly directional towards the front ($\phi = 0^\circ$) and back ($\phi = 180^\circ$) ends, having a maximum value in the direction of $\phi = 180^\circ$. It may also be noted from the patterns in Figure 5 that the magnitude of side lobes decreases as the ratio of a/b increases.

The effect on the radiation patterns due to the change of material of the sheath is considered and shown in Figure 6. These patterns

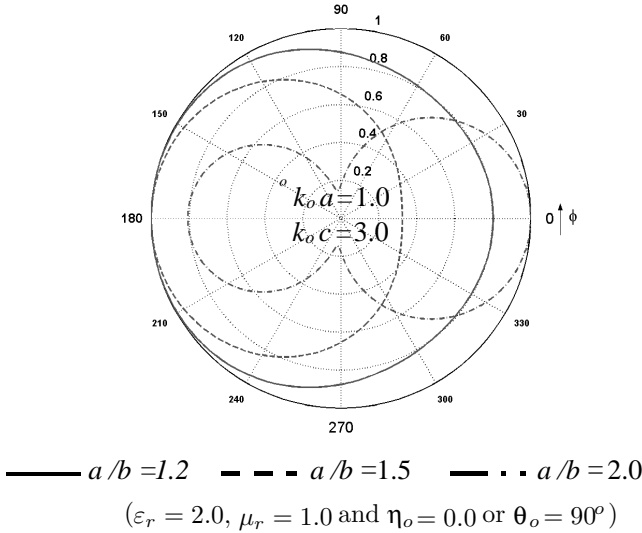


Figure 4. Radiation patterns of a half-wavelength narrow slot antenna located at $\eta_1 = 0$ on perfectly conducting prolate spheroid coated with electric type ($\mu_r = 1.0$) material $\epsilon_r = 2.0$, with the ratios of $a/b = 1.2, 1.5$ and 2.0 , and the electrical lengths of $k_o a = 1$ and $k_o c = 3$.

were obtained from configurations with the same parameters as those given in Figure 5, but with a dielectric constant ϵ_r increased to 4. By comparing Figures 5 and 6, the main beam directions are changed by 180° for the cases $a/b = 1.2$ and 1.5 . This result may be useful in antenna design by coating the antenna with different materials to change the main beam direction.

3.2. Radiated Power

Several investigators [13, 14] have examined the radiation from axially symmetric slot antennas on perfectly conducting spheres coated with homogeneous material. It was found that the thickness of the coating layer has a significant effect on the radiated fields, and the radiated power is greatly enhanced for some values of the thickness. However, this effect has not been studied for either axially symmetric or asymmetric spheroidal slot antennas.

Before performing the investigation for axially asymmetric spheroidal slot antennas, it is desirable to further verify our solution by considering an axially symmetric spheroidal slot antenna with a homogeneous sheath and excited with a delta gap source. This is a

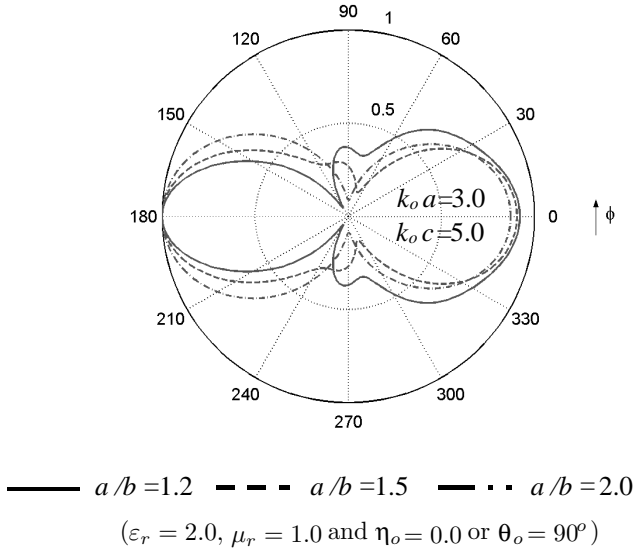


Figure 5. Radiation patterns of a half-wavelength narrow slot antenna located at $\eta_1 = 0$ on perfectly conducting prolate spheroid coated with electric type ($\mu_r = 1.0$) material $\epsilon_r = 2.0$, with the ratios of $a/b = 1.2, 1.5$ and 2.0 , and the electrical lengths of $k_o a = 3$ and $k_o c = 5$.

simplified example of our analysis, and many researchers [13, 14] have investigated its radiation patterns for the special case $a/b \approx 1$.

This simplified antenna model can easily be obtained by extending the slot length from $2L$ (arbitrary length) to the entire circumference to form a complete circular gap on the surface ξ_1 , as illustrated in Figure 7. The excitation source given in (11) over the slot is replaced with a simple delta gap, which is independent of ϕ and can be written as:

$$E_\eta^{ex} = \frac{V_o}{2h_\eta \Delta\eta} \delta(\eta - \eta_1), \tag{34}$$

where V_o is the voltage across the slot, and $h_\eta = F \sqrt{\frac{\xi_1^2 - \eta_1^2}{1 - \eta_1^2}}$. The excitation term given in (29) can then be simplified to:

$$F_{1,N+1}(h_1, \xi_1) = -\frac{V_o k_1}{h_1} \sqrt{(1 - \eta_1^2)} (\xi_1^2 - \eta_1^2) S_{1,N+1}(h_1, \eta_1), \tag{35}$$

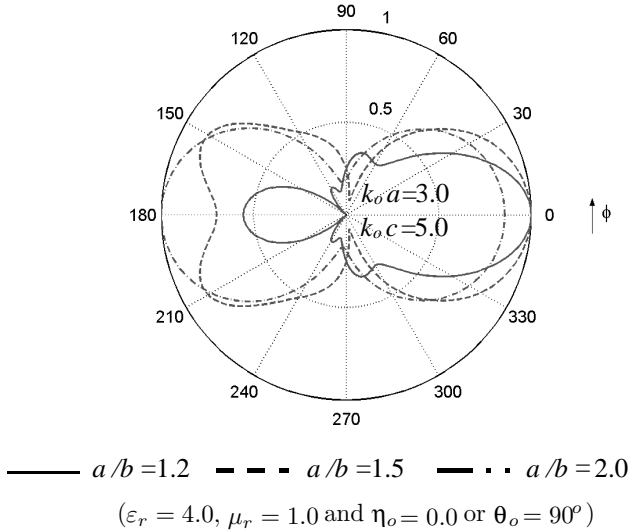


Figure 6. Radiation patterns of a half-wavelength narrow slot antenna located at $\eta_1 = 0$ on perfectly conducting prolate spheroid coated with electric type ($\mu_r = 1.0$) material $\epsilon_r = 4.0$, with the ratios of $a/b = 1.2, 1.5$ and 2.0 , and the electrical lengths of $k_o a = 3$ and $k_o c = 5$.

The total radiated power may be expressed as:

$$P = \frac{1}{Z_o k_o} \sum_{n=0}^{\infty} \sum_{N=0}^{\infty} |\delta_{1n+1}|^2 \cdot \left[\lambda_{11+n}(h_o) I_{101nN}(h_o, h_o) - h_o^2 I_{111nN}(h_o, h_o) \right]. \quad (36)$$

To investigate the effect of the sheath thickness, the radiated power ratio (P/P_o) with and without the sheath (P and P_o respectively) was obtained in terms of the ratio (t/λ_r) of the sheath thickness (t) to the wavelength (λ_r) in the coating materials. Based on the analysis for the axially symmetric slot antenna described above, the radiated power from the spherical slot antenna was calculated by setting $a/b \approx 1$. Some of the results for a range of parameters are presented in Figure 8 for an electric type sheath and in Figure 9 for a magnetic type sheath. It can be seen that for certain sheath thicknesses, the radiated power is greatly enhanced, and becomes resonant. Our results are in an excellent agreement with those of Shafai [13] using spherical wave function analysis. Based on this validation, we explored the effect of the sheath thickness on the radiated power from the axially symmetric and asymmetric spheroidal slot antennas.

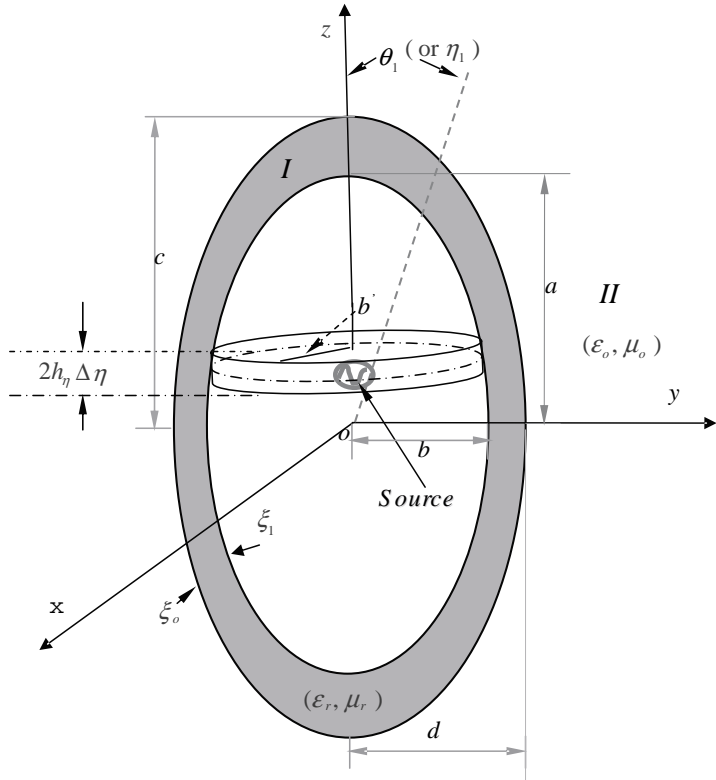


Figure 7. Geometry of axially symmetric slot antenna on a perfectly conducting prolate spheroid with a homogeneous material confocal sheath, a special case of Figure 1.

Figures 10 and 11 show the results for an axially symmetric spheroidal slot antenna. The ratios P/P_o were plotted as functions of the sheath thickness ratio t/λ_r , with varying parameters. The two types of sheaths, the electric (ϵ_r) and magnetic (μ_r) types, have been presented in Figures 10 and 11, respectively. In both Figures, the enhancement in the radiated power becomes more significant as the material constant ϵ_r or μ_r increases. However, with the exception of the resonant points, the radiation power with the magnetic type sheath is always smaller than that without a magnetic sheath. This is because the magnetic sheath has a larger relative impedance than that of the electric sheath. A further comparison can be made between the results obtained from the spherical and spheroidal antennas to see the effect of the ratio of a/b on the radiated power. The results of

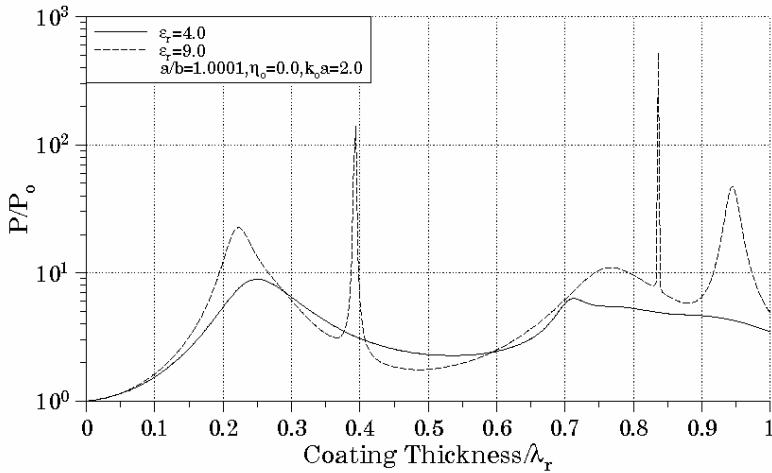


Figure 8. Radiation power of axially symmetric slot spherical antenna (quasi-sphere: $a/b = 1.001$) at $\theta = 90^\circ$ versus the sheath thickness for $k_o a = 2.0$, $\mu_r = 1.0$ and $\epsilon_r = 4.0$ and 9.0 .

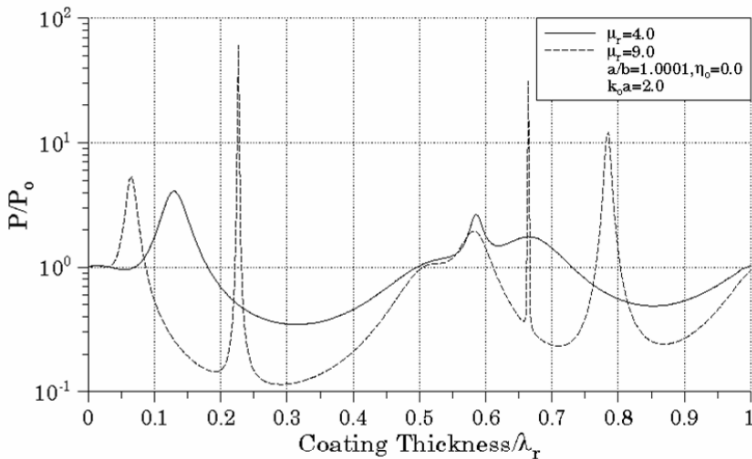


Figure 9. Radiation power of axially symmetric slot spherical antenna (quasi-sphere: $a/b = 1.001$) at $\theta = 90^\circ$ versus the sheath thickness for $k_o a = 2.0$, $\epsilon_r = 1.0$ and $\mu_r = 4.0$ and 9.0 .

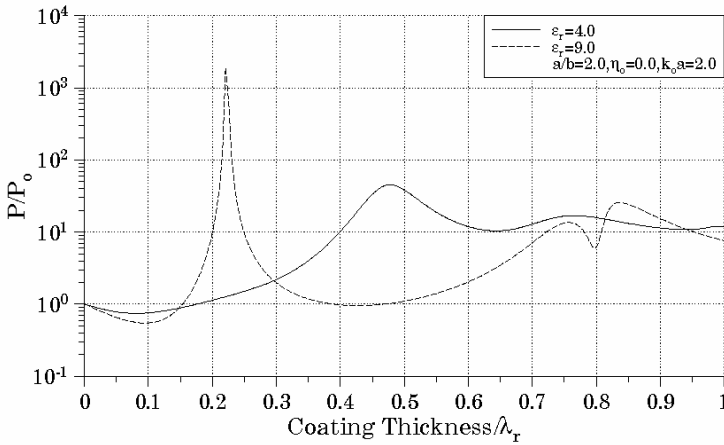


Figure 10. Radiation power of axially symmetric slot spheroidal antenna $a/b = 2.0$ at $\eta_1 = 0$ (or $\theta = 90^\circ$ versus the sheath thickness for $k_0 a = 2.0$, $\mu_r = 1.0$ and $\epsilon_r = 4.0$ and 9.0 .

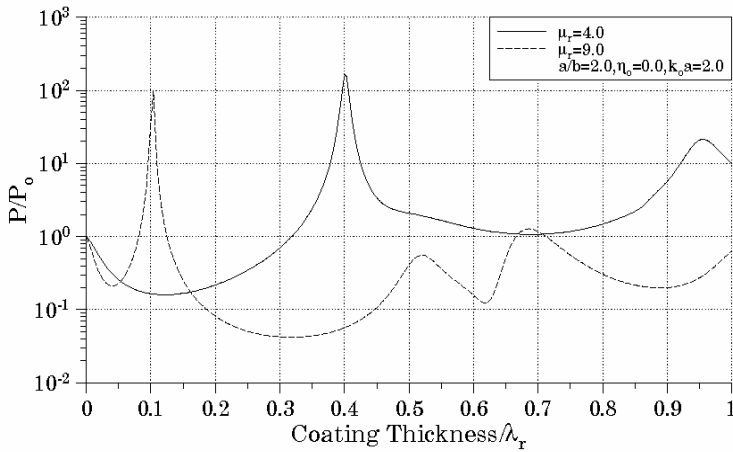


Figure 11. Radiation power of axially symmetric slot spheroidal antenna $a/b = 2.0$ at $\eta_1 = 0$ (or $\theta = 90^\circ$ versus the sheath thickness for $k_0 a = 2.0$, $\epsilon_r = 1.0$ and $\mu_r = 4.0$ and 9.0 .

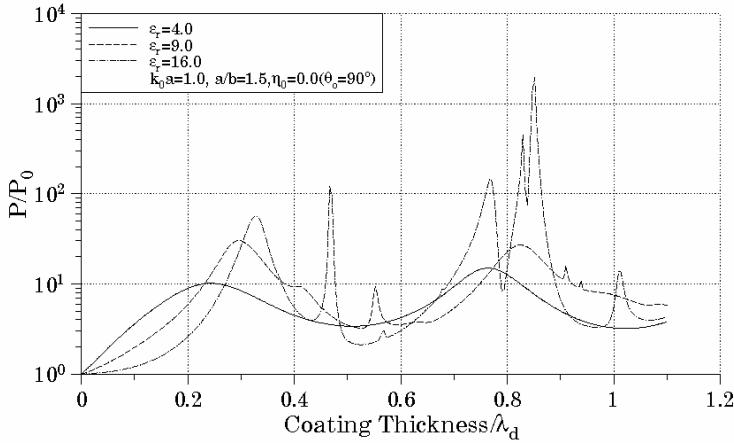


Figure 12. Radiation power of axially symmetric slot spheroidal antenna at $\eta_1 = 0$ (or $\theta = 90^\circ$) versus the sheath thickness for $k_0 a = 1.0$, $a/b = 1.5$, $\mu_r = 1.0$ and $\epsilon_r = 4.0$, 9.0 and 16.0 .

the spherical antenna, as given in Figures 8 and 9, display higher and narrower resonant peaks, and occurring more frequently compared to the corresponding spheroidal antenna cases as shown in Figures 10 and 11. This is mainly due to the propagation of surface wave in the sheath region and is similar that reported by Richmond [15] for coated elliptic cylinders. He stated that an elliptic cylinder with a small a/b value (slightly away from circular cylinder in shape) is related to a nearly uniform sheath in thickness. The surface wave can propagate all the way around the perimeter of the elliptic cylinder with very small attenuation, such that the resonant peaks of radiated power are high and narrow. Otherwise, for an elliptic cylinder with a larger a/b value, the sheath thickness is highly varying, and the surface wave propagating through the cylinder experiences a large attenuation with the wave resonance significantly damped.

For the more general case of axially asymmetric slot antenna, the power ratios are plotted in terms of the thickness of the coating sheath and shown here as Figures of 12 to 14 for three parameter combinations. Figures 12 and 13 show the effect of the coating material for two different values of a/b . Although in both Figures the results show that increasing the dielectric constant ϵ_r from 4 to 16 significantly enhances the resonance, this effect can be greatly reduced by increasing the ratio a/b values. Again, it can be seen that the resonant peaks shown in Figure 12 with a smaller ratio of $a/b = 1.5$ are sharper and

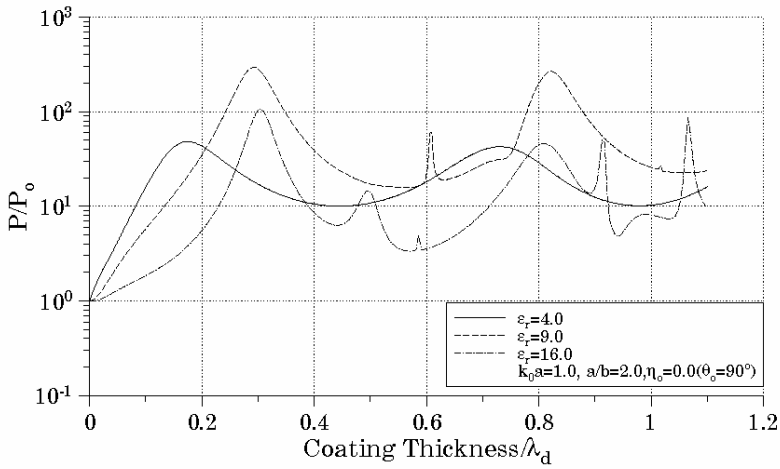


Figure 13. Radiation power of axially symmetric slot spheroidal antenna at $\eta_1 = 0$ (or $\theta = 90^\circ$ versus the sheath thickness for $k_0 a = 1.0$, $a/b = 2.0$, $\mu_r = 1.0$ and $\epsilon_r = 4.0, 9.0$ and 16.0 .

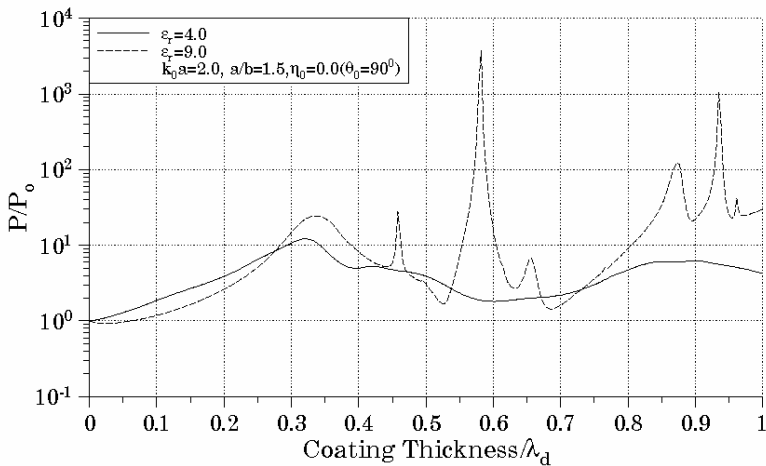


Figure 14. Radiation power of axially symmetric slot spheroidal antenna at $\eta_1 = 0$ (or $\theta = 90^\circ$ versus the sheath thickness for $k_0 a = 2.0$, $a/b = 1.5$, $\mu_r = 1.0$ and $\epsilon_r = 4.0$ and 9.0 .

higher than those in Figure 13 with a larger ratio of $a/b = 2.0$. This behavior is mainly due to the nearly- and non-uniform sheath thickness in Figures 12 and 13, respectively, as reported by Richmond [15] for the coated elliptic cylinder case.

Figure 14 shows the effect on the resonance due to increasing electric size k_0a to 2 while the other parameters used in Figure 12 are unchanged. By comparing Figures 12 and 14, it can be seen that with a higher k_0a the resonant peaks are more significant. This situation is quite similar to that of the axial slot spherical antenna with coating layer investigated by Shafai [13].

4. CONCLUSION

An analytical solution to the problem of electromagnetic radiation from an axially asymmetric prolate spheroidal antenna with a confocal homogeneous lossless electric or magnetic material sheath has been obtained. The problem is solved using the technique of separating the vector wave equation in prolate spheroidal coordinates. The radiated and transmitted fields were expanded in terms of the prolate spheroidal vector wave functions and the expansion coefficients were determined by applying the boundary conditions and the excitation field. Numerical results were obtained for the near field, radiation pattern and total radiated power. The validity and accuracy of the numerical results were examined for both near and far fields.

Numerical calculations have been carried out with various design parameters, e.g., the material constants and thickness of the sheath, the shape and size of the antenna and sheath, to investigate the effect of the parameters on the radiation patterns and power. This investigation showed that the geometrical shape and size of the antenna and the dielectric constant have significant effects on the radiation pattern. Our results also showed that for certain thickness of the sheath, high and sharp resonant peaks appear in the radiated power. In general, increasing the dielectric or magnetic constant ϵ_r or μ_r has a significant effect of enhancing the resonance, but this effect can be greatly reduced by increasing the axial ratio of semi-major axis to semi-minor axis. This conclusion is consistent with that obtained by investigating the axial slot antenna on a dielectric-coated elliptic cylinder as reported by Richmond [15].

REFERENCES

1. Wait, J. R., "Electromagnetic radiation from spheroidal structures," *Advanced Antenna Theory*, R. E. Collin and F. J. Zucker

- (eds.), Part I, Ch. 13, 523–559, McGraw-Hill, New York, 1969.
2. Schelkunoff, S. A., *Advanced Antenna Theory*, John Wiley & Sons, Inc., New York, 1962.
 3. Weeks, W. L., *Electromagnetic Theory for Engineering Applications*, John Wiley & Sons, Inc., New York, 1964.
 4. Wait, J. R., “Theories of prolate spheroidal antenna,” *Radio Sci.*, Vol. 1. No. 4, April 1966.
 5. Do-Nhat, T. and R. H. MacPhie, “The input admittance of the thin prolate spheroidal dipole antenna with finite gap width,” *IEEE Trans. Antennas Propagation*, 1243–1252, Nov. 1995.
 6. Li, L. W., M. S. Lenong, T. S. Yeo, and Y. B. Gan, “Electromagnetic radiation from a prolate spheroidal antenna enclosed in a confocal spheroidal radome,” *IEEE Trans. Antennas Propagation*, Vol. 50, 1525–1533, Nov. 2002.
 7. Zhang, M. and A. A. Sebak, “Radiation characteristics of a slot antenna on a conducting prolate spheroid,” *Canadian J. Phys.*, Vol. 73, 376–385, 1995.
 8. Flammer, C., *Spheroidal Wave Functions*, Stanford University Press, Stanford, California, 1957.
 9. Zhang, M., “Radiation characteristics of asymmetrically slotted spheroidal antennas,” Master Thesis, The University of Manitoba, Winnipeg, Manitoba, Canada, Jan. 1995.
 10. Sinha, B. P. and R. H. MacPhie, “Electromagnetic scattering by prolate spheroids for plane waves with arbitrary polarization and angle of incidence,” *Radio Sci.*, Vol. 12. No. 2, 171–184, March 1997.
 11. Sebak, A. A. and B. P. Sinha, “Scattering by a conducting spheroidal object with dielectric coating at axial incidence,” *IEEE Trans. Antennas Propagation*, Vol. 40, 268–274, March 1992.
 12. Mushiake, Y. and R. E. Webster, “Radiation characteristics with power gain for slot on a sphere,” *IRE Trans. Antennas Propagation*, Vol. 5, 47–55, Jan. 1957.
 13. Shafai, L. and R. H. Chugh, “Resonance effects in slotted spherical antenna coated with homogeneous materials,” *Canadian J. Phys.*, Vol. 51, 2341–2346, 1973.
 14. Lin, C. C. and R. E. Mu, “Improved radiation from a spherical antenna by overdense plasma coating,” *IEEE Trans. Antennas Propagation*, Vol. 17, 675–678, Sept. 1969.
 15. Richmond, J. H., “Axial slot antenna on dielectric-coated elliptic cylinder,” *IEEE Trans. Antennas Propagation*, Vol. 37, 1235–1241, Oct. 1989.